Resistive Collimation of Electron Beams in Laser-Produced Plasmas

A. R. Bell and R. J. Kingham
Blackett Laboratory, Imperial College, London SW7 2AZ, United Kingdom
(Received 11 July 2002; published 17 July 2003)

Intense relativistic electron beams, produced by high-intensity short-pulse laser irradiation of a solid target, have many potential applications including fusion by fast ignition. Using a unique Fokker-Planck code, supported by analytic calculations, we show that fast electrons can be collimated into a beam even when the fast electron source is not strongly anisotropic, and we derive a condition for collimation to occur.

DOI: 10.1103/PhysRevLett.91.035003 PACS numbers: 52.50.Jm, 52.38.Fz, 52.65.Ff

Dramatic progress in the development of short-pulse high-intensity lasers has led the physics of laser-plasma interactions into completely new regimes. At present laser intensities, now exceeding 10^{19} W cm^{-2}, electrons in the laser beam oscillate relativistically. When the laser is focused onto the surface of a solid, large numbers of energetic electrons are produced which interact to produce copious MeV photons [1] and MeV ions [2] that have many potential applications [3]. These conditions are relevant to inertial confinement fusion (ICF) by fast ignition [4], for which the collimation of electron beams, as discussed here, may have substantial benefit.

Recent experiments have shown that irradiation of solid targets at these high intensities with short laser pulses produces intense beams of highly collimated energetic electrons [5]. The "fast electrons" have mean free paths larger than the typical thickness of the solid target and collision times longer than the duration of the laser pulse. Under these conditions, the fast electrons might be expected to flood the target, but it is found experimentally that they penetrate the target as a beam. Numerical simulations by Davies *et al.* [6] have reproduced this effect through the generation of magnetic field, and Gremillet *et al.* [7] have shown that magnetic field can act further to filament the beam. In this Letter, we derive the conditions for collimation to take place, derive approximate equations for important parameters, and demonstrate that collimation can occur even when the fast electron source is not strongly anisotropic. We show that the target Z is an important parameter, that typical experiments only just enter the regime for beam generation, and that the conditions for beam generation depend on some experimental parameters with an opposite dependence to that which might be expected. We demonstrate beam collimation using a recently developed Fokker-Planck code which, as in Ref. [8], is two dimensional and includes magnetic field, but takes the further step of modeling the electron distribution to any required degree of anisotropy by the use of a spherical harmonic expansion which is the multidimensional equivalent of the Legendre polynomial expansion used in Ref. [9].

As a baseline comparison for the simulation, we first derive an approximate analytic model in which the fast electrons, with a characteristic energy $eT_{\rm fast}$, are generated within the solid target and near the target surface in a hemisphere with a radius equal to the radius $R_{\rm laser}$ of the laser spot. The fast electrons emerge from the hemisphere partially collimated with a half angle $\vartheta_{1/2}$ according to the laser absorption process. As the fast electrons enter the ambient solid density plasma they set up an electric field E due to charge separation. The electric field opposes the current $j_{\rm fast}$ of fast electrons, and draws a return current $j_{\rm cold} = E/\eta$ of cold electrons that balances the electric current of fast electrons where η is the resistivity of the cold plasma [10]. Quasineutrality and induction require that to a good approximation $j_{\rm fast} = -j_{\rm cold}$ [11]. B is the magnetic field generated according to $\partial B/\partial t = -\nabla \times E = \nabla \times (\eta j_{\rm fast})$ when resistive diffusion is neglected. The magnetic field is azimuthal around the fast electron beam and acts to collimate it. If the radius of the beam is R, we can estimate the magnetic field by $\partial B/\partial t = \eta j_{\rm fast}/R$, where the resistivity is that given in Ref. [12] apart from multiplication by $1.25Z$ to account approximately for angular scattering by both electrons and ions. The return current drawn by the electric field ohmically heats the background plasma, $(3/2)ne(\partial T_{\rm cold}/\partial t) = \eta j_{\rm fast}^2$. The fast electron current is given by $j_{\rm fast} = I/T_{\rm fast}$ where I is the electron beam intensity. Integration gives $B_{\rm MG} = 0.38 n_{23} P_{\rm TW}^{-1} T_{511} R_{\mu\rm m}(T_{c,\rm keV} - T_{i,\rm keV})$ and $T_{c,\rm keV} = (80 n_{23}^{-1} Z \ln\Lambda P_{\rm TW}^2 T_{511}^{-2} R_{\mu\rm m}^{-4} t_{p\rm sec} + T_{i,\rm keV}^{5/2})^{2/5}$, where $B_{\rm MG}$ is the magnetic field in MG, $P_{\rm TW}$ is the power in the fast electron beam ($P = I\pi R^2$) in TW, n_{23} is the electron density in units of 10^{23} cm^{-3}, T_{511} is the fast electron temperature $T_{\rm fast}$ in units of 511 keV, $R_{\mu\rm m}$ is the beam radius in units of μm, $t_{\rm psec}$ is the time in psec, $T_{c,\rm keV}$ is the temperature ($T_{\rm cold}$) of the cold background plasma in keV, and $T_{i,\rm keV}$ is the initial value ($T_{\rm init}$) of $T_{\rm cold}$ in keV.

The ability of the magnetic field to collimate the fast electrons is determined by the ratio of the beam radius R to the fast electron Larmor radius r_g. Collimation occurs if $R/r_g > \vartheta_{1/2}^2$, in which case the magnetic field is sufficient to bend the fast electron trajectory through an angle

$\vartheta_{1/2}$ in the distance $R/\vartheta_{1/2}$ in which the beam radius approximately doubles. The condition for collimation is that $\Gamma > 1$ where $\Gamma = 0.022 n_{23} P_{\rm TW}^{-1} R_{\mu\rm m}^2 T_{511}^{1/2} (2 + T_{511})^{-1/2} (T_{c,\rm keV} - T_{i,\rm keV}) \vartheta_{\rm rad}^{-2}$ and $\vartheta_{\rm rad}$ is $\vartheta_{1/2}$ in radians.

In the limit of substantial resistive heating ($T_{\rm cold} \gg T_{\rm init}$), the equations reduce to

$$T_{c,\rm keV} = 5.8 n_{23}^{-2/5} Z^{2/5} \ln\Lambda^{2/5} P_{\rm TW}^{4/5} T_{511}^{-4/5} R_{\mu\rm m}^{-8/5} t_{\rm psec}^{2/5},$$

$$B_{\rm MG} = 2.2 n_{23}^{3/5} Z^{2/5} \ln\Lambda^{2/5} P_{\rm TW}^{-1/5} T_{511}^{1/5} R_{\mu\rm m}^{-3/5} t_{\rm psec}^{2/5},$$

$$\Gamma = 0.13 n_{23}^{3/5} Z^{2/5} \ln\Lambda^{2/5} P_{\rm TW}^{-1/5} T_{511}^{-3/10} \times (2 + T_{511})^{-1/2} R_{\mu\rm m}^{2/5} t_{\rm psec}^{2/5} \vartheta_{\rm rad}^{-2}.$$

The inverse dependence of Γ on the fast electron energy $T_{\rm fast}(T_{511})$ is due to the smaller number of fast electrons, and hence the lower current $j_{\rm fast}$, needed to carry the beam energy if $T_{\rm fast}$ is large. Most of the dependences are weak because the collimation process is self-limiting through the decrease of the resistivity as the target is heated. The importance of the resistivity, through its temperature dependence, also causes the surprising result that collimation is favored by low beam power, although the dependence is only weak. Collimation is weaker if the beam power is large because more rapid heating of the cold plasma reduces the resistivity and hence reduces the magnitude of the electric field needed to draw the return current. In the opposite limit of weak resistive heating ($T_{\rm cold} \sim T_{\rm init}$), in which the background heating is dominated by other heating processes, the equations reduce to $B_{\rm MG} = 12 Z \ln\Lambda P_{\rm TW} T_{511}^{-3/2} R_{\mu\rm m}^{-3} T_{i,\rm keV}^{-3/2} t_{\rm psec}$ and $\Gamma = 0.7 Z \ln\Lambda P_{\rm TW} T_{511}^{-3/2} (2 + T_{511})^{-1/2} R_{\mu\rm m}^{-2} T_{i,\rm keV}^{-3/2} t_{\rm psec} \vartheta_{\rm rad}^{-2}$. The self-limiting effect due to resistive heating no longer applies, so the dependences follow intuition more closely, although the inverse dependence on $T_{\rm fast}(T_{511})$ remains for the same reason as in the limit of substantial heating.

In all cases, collimation is stronger in high Z targets because of their higher resistivity. Hatchett *et al.* [13] have found differences between the ion beams produced by high and low Z targets, but it is not clear whether this connects with the phenomena investigated here. The strongest dependence in the condition for collimation is that on the anisotropy of the source of fast electrons. Γ is inversely proportional to the square of the half angle $\vartheta_{1/2}$ of the cone of generation. Hence, collimation occurs more easily if the fast electrons are generated with some degree of beaming into the target. Our estimates of the condition for collimation apply only if the temperature of the cold electrons is raised into the regime in which the Spitzer conductivity applies. This condition is violated at low intensities at which strong jet formation does not occur [14]. Furthermore, effects such as microstabilities and Weibel instability within the beam are not considered and may disrupt beam formation.

We investigated the collimation process using a recently developed relativistic Fokker-Planck (FP) code with unique capabilities, named KALOS (kinetic laser-plasma simulation). All electrons, both fast and cold, are treated as part of the same population. This contrasts with hybrid simulations by Davies *et al.* [6] and by Gremillet *et al.* [7]which treated the fast electrons kinetically as particles and the cold electrons nonkinetically as a background medium with a temperature and resistivity. An FP code overcomes the incorrect assumptions made in hybrid codes that the fast and cold electrons are distinct populations, and that nonlocal and non-Maxwellian effects are unimportant for cold electrons and electrons with intermediate energies. We treat the ions as a stationary fluid with constant Z, thus ignoring ionization. The code is two dimensional and cylindrical in space and three dimensional in momentum. Momentum space is represented by a grid in magnitude of momentum, with the angular coordinates (ϑ, ϕ) represented by an expansion in spherical harmonics. The distribution function is written as a sum over terms of the form $f_n^m(r, z, p, t) P_n^m(\cos\vartheta) e^{im\varphi}$.

The electron-electron collision term is expressed in the usual way in terms of Rosenbluth potentials, but the potentials are calculated only from the isotropic part of the electron distribution. This is acceptable because the effect of electron-electron collisions is smaller by a factor Z than that of electron-ion collisions and because electron-electron scattering is dominated by the deflection of electrons by the large numbers of cold electrons that are nearly isotropic in distribution. The electron-electron and electron-ion collision terms are included for all parts (all n and m) of the electron distribution. The full Maxwell equations are solved with the magnetic field calculated from $\partial B/\partial t = -\nabla \times E$. The electric field, obtained through the equation $\partial E/\partial t = c^2 \nabla \times B - j/\varepsilon_0$, is calculated either implicitly or explicitly. If E is calculated explicitly, j is multiplied by a numerical factor, as in Ref. [9], to make the plasma frequency smaller than 1 over the time step, but the results are the same as for the implicit calculation since Langmuir oscillations are unimportant. Collisions are always treated implicitly. All other parts of the code are explicit. KALOS can be understood as a $2\frac{1}{2}$-dimensional equivalent of the code in Ref. [9], except that the current instead of the charge density is used as the source for the electric field. Equally, it can be understood as a finite difference equivalent of a particle-in-cell (PIC) code with collisions added. The small explicit time step, typically around 0.5–1 fsec, is offset by the simplicity of the explicit scheme, giving a code that is robust and rapid in execution. Values of f_n^m for odd and even n are stored on separate grids in p which are displaced from each other by half a momentum step $\Delta p/2$. This makes the calculation more complicated in (r, z), but facilitates use of a well-differenced leapfrog scheme in the more demanding momentum calculation.

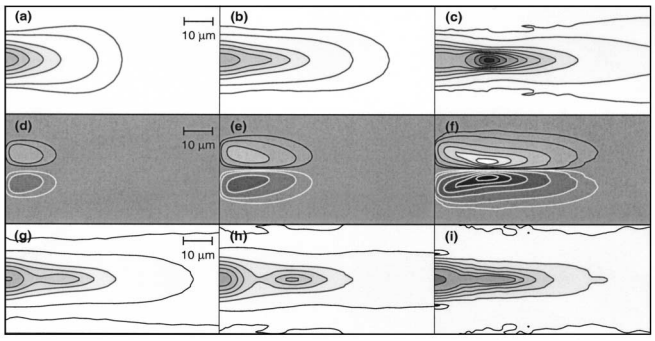

FIG. 1. Spatial plots (close to the axis) of temperature (a)–(c) and (g)–(i) for parameters given in Table I. (d)–(f), respectively, plot the magnetic field for cases (a)–(c). The temperature contour levels are 350, 400, 600, 800, 1000, 1200, 1400, 1800, 2200, and 2600 eV. The magnetic field contour levels are $+/-$ 0.1, 0.2, 0.5, 1.0, 1.5, and 2.0 MG.

Reflective boundaries are used throughout, and reflection at the large z boundary mimics the reflection of electrons by the electric field at the rear of the target. Laser energy is absorbed with a cosine squared spatial dependence ($\cos^2[\pi\sqrt{r^2+z^2}/4R_{\rm laser}]$) into the plasma in a hemispherical region of radius $R_{\rm laser}$ at the $z=0$ boundary. Absorption is modeled each time step by removing a fraction of electrons at all momenta and replacing them with the same number of electrons with a specified distribution $f_{\rm fast} \propto (p_z/p)^N p^4[\exp(-p^2/2p_f^2)]$ where p_f is chosen to give the required mean injected fast electron energy $eT_{\rm fast}$. N determines the anisotropy of the injected electrons, such that, in the limit of large N, the half-height half angle of the distribution is $\vartheta_{1/2} = 1.18/\sqrt{N}$ rad $= 67°/\sqrt{N}$.

Results obtained with KALOS are displayed in Fig. 1 and Table I. Figures 1(a)–1(c) plot the energy density for the standard run (run A) close to the $r=0$ axis. The energy density is expressed as a temperature T (the density is uniform), defined such that the electron energy density, summed over all electrons, is $3nkT/2$. Figures 1(d)–1(f) plot the magnetic field for run A. The rate at which fast electrons are injected is constant in time with a value such that the average absorbed power is in the region of 1 TW and the absorbed laser intensity is accordingly in the region of 10^{18} W cm^{-2}. For run A, $\ln\Lambda = 2$, $T_{\rm fast} = 300$ keV, $Z = 10$, $n = 5\times10^{23}$ cm^{-3}, $N = 10$, $\vartheta_{1/2} = 21°$, $R_{\rm laser} = 5$ μm, and the initial electron temperature is 300 eV. The target thickness is 75 μm represented by a reflective boundary at this distance, and the lateral boundaries in r are placed 37.5 μm from the center of the laser spot. Because N is even, fast electrons are injected both moving away from and moving towards the boundary at $z=0$ where they are reflected towards positive z. The expansion in spherical harmonics is taken to 15th order. This is sufficient to allow for any increase in the degree of anisotropy beyond that ($N=10$) imposed through the fast electron source. A lack of jet formation when the magnetic field is switched off confirms that magnetic field is a crucial part of the process. In the standard run, Fig. 1(a) shows that a jet is just beginning to form after 200 fsec. Figure 1(d) shows the generation of magnetic field around the current of fast electrons at the same time. Figure 1(b) shows that a strong jet is forming by 400 fsec, by which time the magnetic field has grown to 0.8 MG. The corresponding fast electron Larmor radius of 25 μm is sufficiently small to collimate the fast electrons into a jet. By 800 fsec, the maximum magnetic field has further grown to 2.4 MG. This is sufficient to strongly focus the fast electrons into a very well collimated jet. Indeed, the magnetic field now overfocuses the beam, causing a very high density of fast electrons at the point indicated by the peak in the temperature in Fig. 1(c). The fast electrons can only escape along the axis through a narrow null in the magnetic field. Nevertheless, these propagating fast electrons continue as a jet which reaches the far computational boundary at a distance of 75 μm from the front surface. Figure 2 shows that the maximum magnetic field in the simulation begins to grow more rapidly at 600 fsec when strong focusing sets in, thus initiating a positive feedback between a growing magnetic field and a narrowing jet.

Figure 2 compares the magnetic field calculated by KALOS with the field estimated with the approximate analytic model (using the formula for general $T_{\rm init}$) with different initial temperatures $T_{\rm init} = 0.5$ keV and $T_{\rm init} =$

TABLE I. Parameters for Fig. 1. Power is the average absorbed power up to that time. $T_{\rm max}$ and $B_{\rm max}$ are calculated by KALOS. $B_{\rm est}$ and F are given by the approximate analytic model with $T_{\rm init} = 1.5$ keV.

Figure	Run	Time fsec	Power TW	$T_{\rm max}$ keV	$B_{\rm max}$ MG	$B_{\rm est}$ MG	Γ	Conditions
(a),(d)	A	200	2.1	1.4	0.4	0.5	0.8	Standard
(b),(e)	A	400	1.9	1.3	0.8	0.9	1.6	Standard
(c),(f)	A	800	1.5	2.8	2.4	1.7	2.9	Standard
(g)	B	1200	1.3	1.4	1.5	2.2	1.5	$\vartheta_{1/2} = 33°$
(h)	C	2500	0.8	1.5	1.8	2.9	1.1	$\vartheta_{1/2} = 45°$
(i)	D	1500	1.2	2.0	0.9	0.7	0.9	Vary $T_{\rm fast}$, Z, n

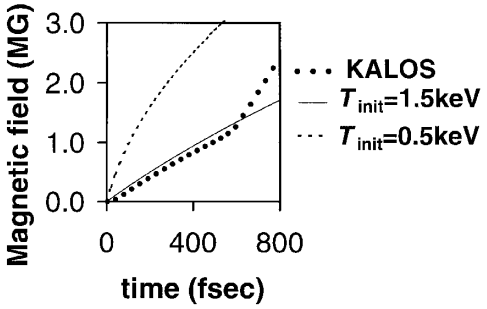

FIG. 2. Time dependence of the maximum magnetic field calculated by KALOS and the value estimated by the approximate calculation with $T_{\text{init}} = 0.5$ keV and $T_{\text{init}} = 1.5$ keV.

1.5 keV. In the analytic calculations, $P_{\text{TW}} = 1.5$ (the average over 800 fsec). The poor agreement for $T_{\text{init}} = 0.5$ keV indicates that, by the time magnetic field generation starts, the temperature of the thermal plasma just beyond the heated region is much higher than its initial value of 300 eV. This is not surprising since it will be heated by thermal conduction out of the heated region during the initial period when the population of fast electrons is building up and when the fast electron propagation is inhibited by space-charge electric fields [10]. The fast initial rise in magnetic field when $T_{\text{init}} = 0.5$ keV is caused by the high resistivity at this low temperature. In contrast, when T_{init} is set equal to a value (1.5 keV) typical of the heated plasma, the model gives excellent agreement with KALOS until focusing sets in at 600 fsec. The values of B_{est} and Γ given in Table I for all runs (*B–D* as well as *A*) are calculated for $T_{\text{init}} = 1.5$ keV. Comparison with results from KALOS supports $\Gamma > 1$ as a useful approximate condition for beam formation, although the condition is sensitive to the choice of T_{init}.

Runs *B–D*, Figs. 1(g)–1(i), vary the parameters from the standard parameters as indicated in Table I. Runs *B* and *C* demonstrate that a jet forms even when the fast electrons are injected with wide half angles of 33° and 45°. In these cases, the jet forms later in time as expected from our approximate calculation that showed a relatively strong dependence of Γ on $\vartheta_{1/2}$, but the beam, when formed, is narrow. Run *D* shows that jet formation follows the same pattern when other parameters are varied. In run *D*, $T_{\text{fast}} = 500$ keV, $Z = 4$, $n = 3 \times 10^{23}$ cm^{-3}, and other parameters are unchanged from the standard run. For unfavorable simulation parameters, particularly if the angle $\vartheta_{1/2}$ is large, collimation can take longer than a typical experimental pulse length of 1 psec, thus indicating that current experiments may only just enter the regime for beam generation.

In summary, we have demonstrated analytically and numerically that resistive collimation is able to produce a beam of fast electrons propagating into a solid target, that the process is effective even when the source of fast electrons is not strongly anisotropic, that the time scale for beam formation is of the order of 0.5–1 psec for current experimental parameters, and that an approximate analytic condition for collimation represents well the important features of sophisticated numerical simulations.

This work is supported by the U.K. Engineering and Physical Sciences Research Council under Grants No. GR/M38988 and No. GR/R71979.

[1] P. A. Norreys *et al.*, Phys. Plasmas **6**, 2150 (1999); Z.-M. Sheng, Phys. Rev. Lett. **85**, 5340 (2000).
[2] K. Snavely *et al.*, Phys. Rev. Lett. **85**, 2945 (2000); K. Krushelnick *et al.*, Phys. Plasmas **7**, 2055 (2000); A. Maksimchuk *et al.*, Phys. Rev. Lett. **84**, 4108 (2000).
[3] M. Borghesi *et al.*, Phys. Plasmas **9**, 2214 (2002); K. W. D. Ledingham *et al.*, Phys. Rev. Lett. **84**, 899 (2000).
[4] Tabak *et al.*, Phys. Plasmas **1**, 1626 (1994); Key *et al.*, Phys. Plasmas **5**, 1966 (1998); P. A. Norreys *et al.*, Phys. Plasmas **7**, 3721 (2000).
[5] M. Tatarakis *et al.*, Phys. Rev. Lett. **81**, 999 (1998); Borghesi *et al.*, Phys. Rev. Lett. **83**, 4309 (1999); L. Gremillet *et al.*, Phys. Rev. Lett. **83**, 5015 (1999); J. A. Koch *et al.*, Phys. Rev. E **65**, 016410 (2002); Y. T. Li *et al.*, Phys. Rev. E **64**, 046407 (2001); G. Pretzler, T. Schlegel, and E. Fill, Laser Part. Beams **19**, 91 (2001); E. Fill, Phys. Plasmas **8**, 1441 (2001).
[6] J. R. Davies, A. R. Bell, and M. Tatarakis, Phys. Rev. E **59**, 6032 (1999).
[7] L. Gremillet, G. Bonnaud, and F. Amiranoff, Phys. Plasmas **9**, 941 (2002).
[8] R. J. Kingham and A. R. Bell, Phys. Rev. Lett. **88**, 045004 (2002).
[9] A. R. Bell, R. G. Evans, and D. J. Nicholas, Phys. Rev. Lett. **46**, 243 (1981).
[10] A. R. Bell *et al.*, Plasma Phys. Controlled Fusion **39**, 653 (1997); S. M. Guerin *et al.*, Plasma Phys. Controlled Fusion **41**, 285 (1999); F. Pisani *et al.*, Phys. Rev. E **62**, R5927 (2000); K. Wharton *et al.*, Phys. Rev. Lett. **81**, 822 (1998).
[11] A. R. Bell, J. R. Davies, and S. M. Guerin, Phys. Rev. E **58**, 2471 (1998).
[12] J. D. Huba, *NRL Plasma Formulary* (Naval Research Laboratory, Washington, DC, 1994).
[13] S. P. Hatchett *et al.*, Phys. Plasmas **7**, 2076 (2000).
[14] A. J. Mackinnon *et al.*, Phys. Rev. Lett. **88**, 215006 (2002).